LANGMUIR

pubs.acs.org/Langmuir Article

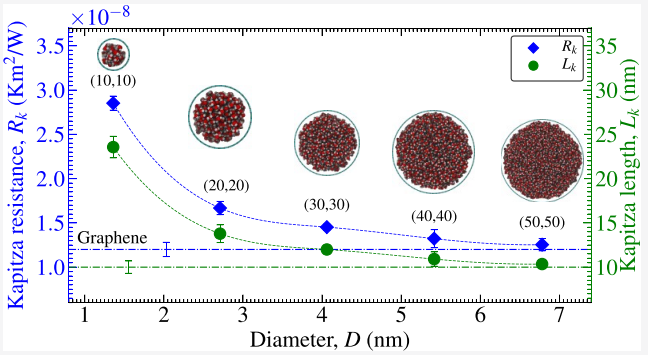
Nanoconfinement Effects on the Kapitza Resistance at Water−CNT Interfaces

Sobin Alosious, Sridhar Kumar Kannam, Sarith P. Sathian, and B. D. Todd*

Cite This: *Langmuir* 2021, 37, 2355−2361 Read Online

ACCESS | Metrics & More | Article Recommendations | Supporting Information

ABSTRACT: The Kapitza resistance (R_k) at the water−carbon nanotube (CNT) interface, with water on the inside of the nanotube, was investigated using molecular dynamics simulations. We propose a new equilibrium molecular dynamics (EMD) method, also valid in the weak flow regime, to determine the Kapitza resistance in a cylindrical nanoconfinement system where nonequilibrium molecular dynamics (NEMD) methods are not suitable. The proposed method is independent of the correlation time compared to Green−Kubo-based methods, which only work in short correlation time intervals. R_k between the CNT and the confined water strongly depends on the diameter of the nanotube and is found to decrease with an increase in the CNT diameter, the opposite to what is reported in the literature when water is on the outside of the nanotube. R_k is furthermore found to converge to the planar graphene surface value as the number of water molecules per unit surface area approaches the value in the graphene surface and a higher overlap of the vibrational spectrum. A slight increase in R_k with the addition of the number of CNT walls was observed, whereas the chirality and flow do not have any impact.



INTRODUCTION

In recent years, graphene and carbon nanotube (CNT)-based materials have exhibited vast potential for resolving nanoscale devices' thermal management obstacles. Suspensions of nanoscale graphene flakes and CNTs in fluids considerably enhance the thermal characteristics of the base fluids.[1] The transport of water through CNTs has drawn significant attention due to their broad range of applications such as water desalination, drug delivery, hydrogen storage, etc.[2−5] In addition to that, the higher Kapitza resistance between water and CNTs can be utilized for effectively transporting liquids at temperatures higher/lower than the ambient temperatures in future nanoscale devices for heating/cooling purposes at specific locations. Studies based on Kapitza resistance in CNT systems were mostly focused on nanocomposites and CNT-based bulk nanofluid systems.[6−10] However, studies on the nanoconfinement effect on Kapitza resistance in systems with water filled inside a CNT and molecular dynamics methods to compute the Kapitza resistance inside such cylindrical nanoconfinement systems are seldom reported to the best of the authors' knowledge.

In this paper, we introduce a novel way to compute the Kapitza resistance/length at the CNT−water interface using both equilibrium molecular dynamics (EMD) and non-equilibrium molecular dynamics (NEMD) simulation techniques. We also study the various factors influencing the Kapitza resistance/length in cylindrical nanoconfinement. The present EMD method is an improved version of our former work, in which we introduced a new method to compute the Kapitza resistance at a planar solid−fluid interface.[11,12] Our EMD method is free from the plateau problem in the EMD method based on the Green−Kubo formalization.[13,14] Using our new method, we examined various factors affecting the Kapitza resistance/length in cylindrical nanoconfinement systems, such as diameter, chirality, the number of walls, and flow. We find that the Kapitza resistance reduces with an increase in the diameter due to an increase in the number of water molecules per unit surface area adjacent to the interface and a higher overlap of the vibrational spectrum. Other parameters, such as the number of walls, chirality, and flow, do not significantly affect the heat transfer at the interface.

THEORY

The derivation for our newly proposed method is given below. It is an improved version from our previous work, in which we now form an autocorrelation function with the kinetic variable (temperature) instead of heat flux, which has both kinetic and (strongly) configuration terms.[11,12] The modified derivation

Received: November 15, 2020
Revised: January 29, 2021
Published: February 11, 2021



Downloaded via UNIV OF NOTRE DAME on July 11, 2026 at 17:15:22 (UTC).
See https://pubs.acs.org/sharingguidelines for options on how to legitimately share published articles.

ACS Publications © 2021 American Chemical Society

https://dx.doi.org/10.1021/acs.langmuir.0c03298
Langmuir 2021, 37, 2355−2361

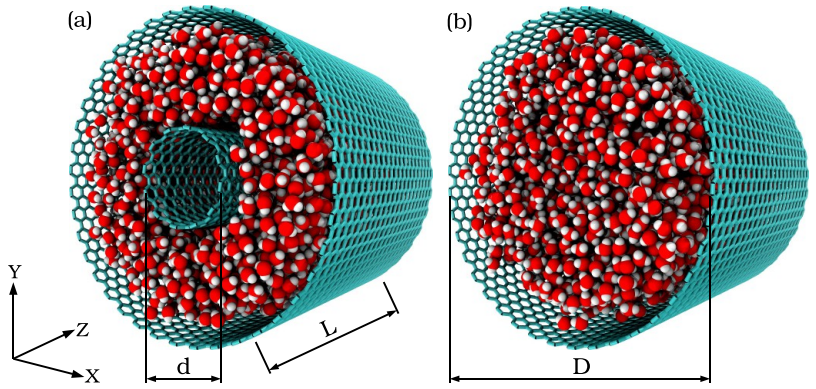


Figure 1. Schematic depiction of the simulation setup. (a) Water filled inside the annular region between two concentric CNTs for the NEMD simulation. (b) Water filled inside a CNT for the EMD simulation.

gives better statistics and a correlation time-independent result and is also recommended for planar interfaces.

The Kapitza resistance or the interfacial thermal resistance, R_k, is defined as

$$R_k = \frac{\Delta T}{J_q} \tag{1}$$

The interfacial thermal conductance, G_k, can be defined as the inverse of R_k

$$G_k = \frac{1}{R_k} = \frac{J_q}{\Delta T} \tag{2}$$

where J_q is the heat flux at the water−CNT interface and $\Delta T = T_f - T_w$ is the difference between the temperature of the CNT, T_w, and a water slab of some small thickness immediately adjacent to the CNT, T_f.

The instantaneous governing constitutive equation can be formulated with regards to the time dependence of the Kapitza kernel at equilibrium as

$$J_q(t) = \int_0^t G_k(t - t')\Delta T(t')\mathrm{d}t' + J_R(t) \tag{3}$$

where $J_R(t)$ is a random heat flux noise term, which is uncorrelated with ΔT with a zero mean, given by

$$\langle J_R(t)\rangle = 0 \text{ and } \langle \Delta T(0) J_R(t)\rangle = 0 \tag{4}$$

Similar to the assumption of Hansen et al.,[15] here, we are assuming that we can neglect nonlocal effects generated by fluid structural inhomogeneity. Multiplying eq 3 by $\Delta T\ (t = 0)$ and calculating the ensemble average gives

$$\begin{aligned}
&\langle \Delta T(0) J_q(t)\rangle \\
&= \left\langle \Delta T(0) \int_0^t G_k(t - t')\Delta T(t')\mathrm{d}t' \right\rangle \\
&= \left\langle \int_0^t G_k(t - t')\Delta T(0)\Delta T(t')\mathrm{d}t' \right\rangle \\
&= \int_0^t G_k(t - t')\langle \Delta T(0)\Delta T(t')\rangle \mathrm{d}t'
\end{aligned} \tag{5}$$

The time-correlation functions can be defined as $C_{TJ_q}(t) \equiv \langle \Delta T\ (0)\ J_q(t)\rangle$ and $C_{TT}(t) \equiv \langle \Delta T\ (0)\ \Delta T(t)\rangle$, so eq 5 can be expressed as

$$C_{TJ_q}(t) = \int_0^t G_k(t - t')C_{TT}(t')\mathrm{d}t' \tag{6}$$

The Laplace transform of some arbitrary function $f(t)$ is defined by

$$L(f(t)) \equiv \int_0^\infty f(t)\mathrm{e}^{-st}\mathrm{d}t \equiv \tilde{f}(s) \tag{7}$$

Note that as a consequence, we have

$$\tilde{f}(s = 0) = \int_0^\infty f(t)\mathrm{d}t \tag{8}$$

which is the steady-state time-independent value of f. Hence, taking the Laplace transform of eq 6 provides

$$\tilde{C}_{TJ_q}(s) = \tilde{G}_k(s)\tilde{C}_{TT}(s) \tag{9}$$

The Kaptiza resistance can now be directly evaluated using eq 9, i.e.,

$$\tilde{G}_k(s) = \frac{\tilde{C}_{TJ_q}(s)}{\tilde{C}_{TT}(s)} \tag{10}$$

from which $G_k \equiv \tilde{G}_k(s = 0)$ can be extracted. However, this procedure is an inefficient way to extract G_k since we are not using the whole data available. So, to obtain a statistically more precise value, we can use all of the available data and deduce $\tilde{G}_k(s)$ by fitting the right-hand side of eq 9 to the left-hand side of the same equation and then directly calculate the value at $s = 0$.

Moreover, if we assume that G_k has a Maxwellian time distribution, as recognized by Hansen et al.,[15] the time dependence of G_k can be expressed as[16]

$$G_k(t) = \sum_{i=1}^{n} k_i \mathrm{e}^{-\mu_i t} \tag{11}$$

where k_i and μ_i are coefficients. Taking the Laplace transform of this gives

$$\tilde{G}_k(s) = \sum_{i=1}^{n} \frac{k_i}{s + \mu_i} \tag{12}$$

Substituting eq 12 into eq 9 gives

https://dx.doi.org/10.1021/acs.langmuir.0c03298
Langmuir 2021, 37, 2355−2361

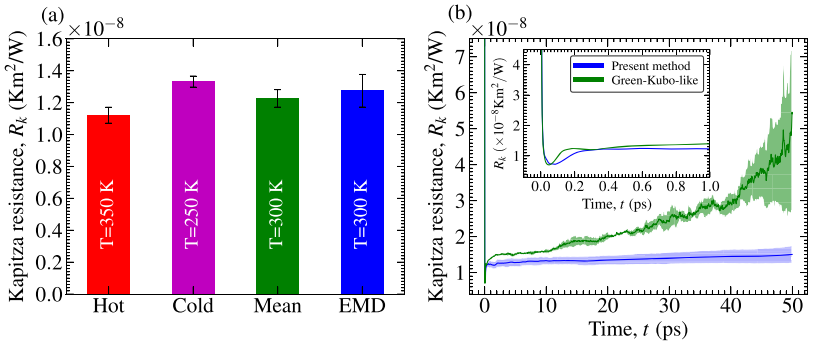


Figure 2. (a) Comparison of the Kapitza resistance obtained from the NEMD and the present EMD methods. (b) Comparison of the Kapitza resistance as a function of correlation time calculated using the present method and the Green−Kubo-like method of Barrat and Chiaruttini.[13,14]

$$\tilde{C}_{\mathrm{TJ_q}}(s) = \sum_{i=1}^{n} \frac{k_i}{s + \mu_i} \tilde{C}_{\mathrm{TT}}(s) \tag{13}$$

Thus, for steady-state conditions ($s = 0$), we have

$$G_{\mathrm{k}} \equiv \tilde{G}_{\mathrm{k}}(0) = \sum_{i=1}^{n} \frac{k_i}{\mu_i} \tag{14}$$

Finally, the Kapitza resistance is obtained as

$$R_{\mathrm{k}} = \frac{1}{G_{\mathrm{k}}} \tag{15}$$

We can extract $C_{\mathrm{TJ_q}}(t)$ and $C_{\mathrm{TT}}(t)$ from EMD simulations. After taking the Laplace transforms, we can fit the right-hand side of eq 13 to the $\tilde{C}_{\mathrm{TJ_q}}(s)$ data with the help of fitting parameters k_i and μ_i. Finally, we calculate the Kapitza resistance from eqs 14 and 15 with the inclusion of these fitting parameters. The instantaneous heat flux at the water−CNT interface, J_{q}, can be calculated using the following equation[17,18]

$$J_{\mathrm{q}}(t) = J_{\mathrm{q}}^{\mathrm{K}}(t) + J_{\mathrm{q}}^{\phi}(t) \tag{16}$$

where $J_{\mathrm{q}}^{\mathrm{K}}(t)$ is the kinetic term and $J_{\mathrm{q}}^{\phi}(t)$ is the potential term of the heat flux.

METHODOLOGY

The simulation domain for the NEMD method is shown in Figure 1a, which consists of water filled inside an annular portion of two concentric CNTs with diameters D = 5.41 nm and d = 1.62 nm (corresponding to chiralities (40,40) and (12,12)). The selection of these particular diameters is described in the Supporting Information. Rigid concentric CNTs were immersed in a large water bath and equilibrated at 300 K temperature and 1 atm pressure. Subsequently, the water molecules except for the annular region were removed. The simulation domain for the EMD method is shown in Figure 1b, which was prepared by immersing a rigid CNT of diameter 5.41 nm in a large water bath and equilibrated at 300 K temperature and 1 atm pressure. The water molecules outside the CNT were removed after the equilibration. Different parameters, such as the number of walls, diameter, chirality, and flow, were varied to study the different confinement variables that affect the Kapitza resistance. The number of CNT walls varied from 1 to 5, and the diameter of the CNT varied from 1.36 to 6.78 nm. CNTs of five different chiralities with similar diameters were chosen. Also, the flow inside the CNT was varied by providing external accelerations ranging from 0 to 5 m/s^2. The modeling aspects are given in the Supporting Information. The water molecules were modeled using the simple point charge (SPC/E)[19,20] water model. The SHAKE[21] algorithm was used to keep the water molecules rigid, and the particle−particle particle−mesh (PPPM)[22] solver was used to compute the long-range electrostatic forces. Periodic boundary conditions were employed in all three directions. To eliminate the errors due to electrostatic interactions between periodic images while implementing the PPPM method, a 5 nm void spacing between periodic images was introduced in the x and y directions.[23] The intralayer carbon interactions were modeled using the adaptive intermolecular reactive empirical bond-order (AIREBO)[24] potential. Also, the interlayer carbon interactions for the multiwall CNT were modeled using a pairwise Lennard−Jones (L−J) potential, $\phi_{ij}(r) = 4\epsilon[(\sigma/r)^{12} - (\sigma/r)^{6}]$ with the parameters σ = 3.414 Å and ϵ = 0.2323 kJ/mol.[25] The carbon−water interactions were modeled by L−J potentials with parameters σ = 3.190 Å and ϵ = 0.3920 kJ/mol.[26] A cutoff distance of 10 Å was set for the short-range Coulombic forces and the L−J potential. The Large-scale Atomic/Molecular Massively Parallel Simulator (LAMMPS)[27] package with a time step of 1.0 fs was employed to perform all of the MD simulations and visual molecular dynamics (VMD)[28] was utilized for visualization.

The simulation procedure involves energy minimization of the entire system, followed by a 2.0 ns equilibration in the canonical (NVT) ensemble. After that, the system stability was verified for another 2.0 ns by simulating under a micro-canonical (NVE) ensemble. For the NEMD simulation, a temperature gradient in water along the radial direction was generated by the addition and subtraction of heat from the inner and the outer CNTs, respectively. The heat addition and subtraction process was achieved by thermostatting the inner and the outer CNTs at different temperatures (350 and 250 K) with the help of a Langevin thermostat.[29] The process of heat addition and removal continued for 6.0 ns until a steady-state heat flux and a linear temperature profile along the radial direction were obtained. The temperature profile and heat flux data were extracted from another 5.0 ns production run. The Kapitza resistance, R_{k}, was computed with the equation $R_{\mathrm{k}} = \Delta T/J_{\mathrm{q}}$, where ΔT is the temperature difference at the water−CNT interface and J_{q} is the heat flux across the interface, which is obtained by computing the energy added/subtracted from the inner and outer CNT per unit time per unit surface area. For the EMD simulations, after checking the system stability, simulations were carried out at an equilibrium temperature of

https://dx.doi.org/10.1021/acs.langmuir.0c03298
Langmuir 2021, 37, 2355−2361

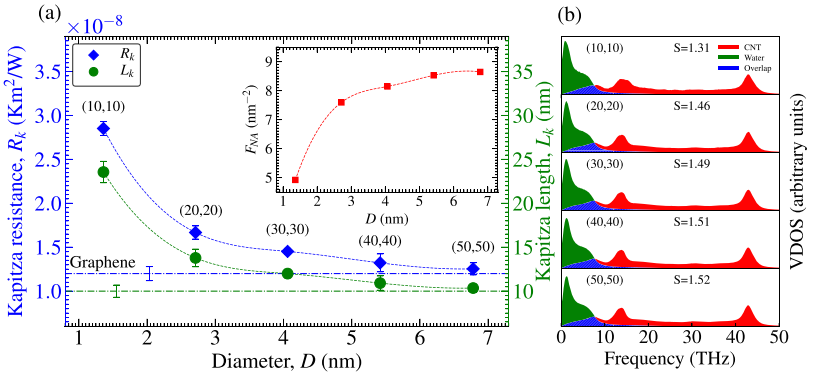


Figure 3. (a) Kapitza resistance/length as a function of the CNT diameter. The horizontal dashed lines correspond to the Kapitza resistance/length at the interface of water confined within a graphene nanochannel[12] and the inset shows the variation of the area density factor, F_{NA}, with the diameter of the CNT. (b) VDOS (arbitrary units) and the overlap, S, of the CNT and the water slab for different diameter CNTs.

300 K for 5.0 ns by thermostatting only the CNT, and the data were extracted. Using the proposed method as described in the Theory section, the Kapitza resistance was calculated with a Maxwellian one term (n = 1) memory function and a fluid slab thickness of Δ = 3.165 Å (the distance measured from the CNT to the first water density peak[30]). Finally, the Kapitza length L_k was calculated using the equation $L_k = R_k\kappa$, where κ is the thermal conductivity of water at 300 K.[12]

RESULTS AND DISCUSSION

Computation of the Kapitza resistance in cylindrical geometry using the NEMD method is limited to a range of CNT diameters, and the simulation system is more complicated than the EMD method. Since the heat transfer takes place between the concentric CNTs with different diameters, the heat flux is not symmetric at both the interfaces. Thus, two separate simulations are required to obtain the mean Kapitza resistance at a particular reference temperature. The radial temperature profile and the NEMD simulation details are provided in the Supporting Information.

A comparison of the Kapitza resistance calculated using both the NEMD and EMD methods is shown in Figure 2a. The NEMD results are the mean of the Kapitza resistance at the outer water−CNT interface corresponding to temperatures of 250 and 350 K. The results obtained from our EMD method are in excellent agreement with the NEMD method results. After validating our EMD method with the results of the NEMD method, all other simulations in this study were performed using our EMD method. The correlation functions and the simulation details of our EMD method are given in the Supporting Information. Barrat and Chiaruttini developed an EMD method based on the Green−Kubo formula to calculate the Kapitza resistance at planar geometry. We compare our EMD method with their method and find that our method is free from the well-known plateau problem in Green−Kubo formalisms for confined fluids.[31] The comparison of the Kapitza resistance as a function of correlation time with our EMD method and the Green−Kubo-like method of Barrat and Chiaruttini[13,14] is shown in Figure 2b. Both the methods match at short correlation time; however, the Green−Kubo-like method diverges with an increase in the correlation time, whereas our EMD method remains nearly independent of the correlation time. Our method makes use of the temperature-difference fluctuation and the heat flux at the interface, thus using more of the data available in the simulation. Furthermore, since the correlation functions are restricted to an interface region of fluid thickness, Δ = 3.165 Å, we can be certain that the Kapitza resistance that we calculate is not a property of the bulk fluid, rather a local interfacial property.[11]

Figure 3a shows the influence of the CNT diameter on the Kapitza resistance/length. The horizontal dashed lines correspond to the Kapitza resistance/length at the interface of water confined within a graphene nanochannel. With the increase in the CNT diameter, the Kapitza resistance monotonically decreases asymptotically to the graphene−water interface value.[11] There was about a 56% reduction in Kapitza resistance when the CNT diameter varied from 1.36 to 6.78 nm, corresponding to chiralities of (10,10) and (50,50), respectively. Alexeev et al.[32] reported that the Kapitza resistance at a planar graphene−water interface is inversely proportional to the first water density peak near the interface. The first water density peak in a CNT is found to be decreasing with an increase in the diameter (see the Supporting Information for the density profile). However, in a CNT, the Kapitza resistance reduces with an increase in the diameter instead of increasing, which is exactly opposite to the findings of Alexeev et al.[32] If we look closely, a higher value of the first density peak indicates a higher number of water molecules near the interface, and thus more heat transfer takes place at the interface leading to a low Kapitza resistance. Thus, the number of molecules per unit surface area of the interface is the deciding factor, and for planar graphene surfaces, the surface area remains the same; therefore, the first density peak is directly proportional to it. However, for a cylindrical geometry, the surface area changes with the diameter, so we cannot purely depend on the first density peak. To quantify this, we introduced a new term called the area density factor, F_{NA}: the ratio of the number of molecules in a slab of fluid adjacent to the interface (wall to the first density peak), N, to the CNT's surface area, A ($F_{NA} = N/\pi DL$).[33] The inset of Figure 3a shows the variation of F_{NA} with the CNT diameter and is found to be increasing with an increase in the diameter. This clearly justifies the reduction in Kapitza resistance with an increase in the diameter as the number of water molecules available near the CNT per unit surface area increases. It is also applicable for planar surfaces since the area remains constant; hence, F_{NA} only depends on the number of molecules in the slab, which is proportional to the first density peak, as reported by Alexeev et al.[32] In addition to that, the Kapitza resistance is found to be increasing with an increase in the hydrophobicity in the planar interface due to the decrease in the area density

https://dx.doi.org/10.1021/acs.langmuir.0c03298
Langmuir 2021, 37, 2355−2361

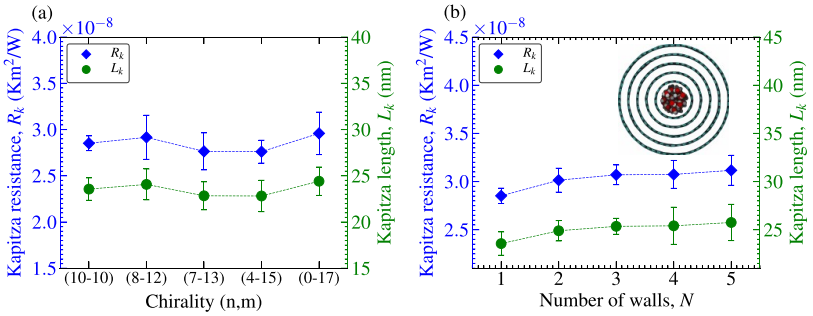


Figure 4. (a) Kapitza resistance/length as a function of CNT chirality for similar diameters. (b) Kapitza resistance/length as a function of the number of CNT walls.

factor or the height of the first density peak.[32,34] For the case of cylindrical geometry, if we consider a CNT with a particular diameter, F_{NA} will decrease with an increase in the hydrophobicity. Since the diameter is constant, F_{NA} and the height of the first density peak are proportional to each other.

We have also assessed the vibrational density of states (VDOS) of the CNT and a water slab adjacent to the wall. The VDOS overlap, S, of the water and the CNT was calculated using the equation[35]

$$S = \frac{\int_0^\infty P(f)_{CNT} P(f)_{water}\, df}{\int_0^\infty P(f)_{CNT}\, df \cdot \int_0^\infty P(f)_{water}\, df} \quad (17)$$

where $P(f)_{CNT}$ and $P(f)_{water}$ are the VDOS of the CNT and water slab, respectively. The calculation of the VDOS is described in the Supporting Information. Figure 3b shows the VDOS (arbitrary units) of the CNT and the water slab for different diameter CNTs and their overlap, S. The vibrational spectrum overlap increases with an increase in the diameter. It shows that a better vibrational coupling between water and CNT at higher diameters, which increases the interface heat transfer, leads to a reduced Kapitza resistance. Jabbari et al.[9] reported an increase in the Kapitza resistance with an increase in the CNT diameter in a water−CNT nanofluid system, where the water is outside the CNT. This can also be explained in terms of the area density factor. If the water is outside the CNT, F_{NA} will be higher for smaller diameters (the trend will be reversed if the water is inside the CNT), leading to a better heat transfer and reduced Kapitza resistance. Thus, by combining these findings, we can infer that the Kapitza resistance is a function of the CNT diameter so that it decreases with an increase in the diameter if the water is inside the CNT and vice versa if the water is outside the CNT.

The effect of the CNT chirality on the Kapitza resistance is shown in Figure 4a. Five different chiralities of (10,10), (8,12), (7,13), (4,15), and (0,17) with similar diameters (<5% difference with a mean diameter of 1.36 nm) were used in this analysis. There is no noticeable change in Kapitza resistance with the chirality of CNTs. In contrast, Sam et al.[36] reported a variation in the friction coefficient and slip length with respect to change in chirality. They observed the highest slip length for armchair (10,10) CNT and lowest in the zigzag (0,17) CNT. This variation in the flow rate is attributed to the difference in potential energy landscape experienced by the water molecules due to change in the CNT structure, leading to a change in the friction coefficient. An analogy between the Kapitza length and slip length can be visible due to the similarity in the effect of different influencing parameters on both. However, the impact of chirality on the slip length and Kapitza length is not identical. The change in the potential energy landscape due to the chirality is observed only in the axial flow direction, whereas the heat transfer happens in the radial direction. Thus, the Kapitza resistance and heat transfer between CNT and water are essentially independent of the CNT's chirality. Figure 4b shows the change in Kapitza resistance as a function of the number of CNT walls. The inset shows the schematic diagram of a multiwalled CNT with five layers. It is found that the number of CNT walls does not have a significant impact on the Kapitza resistance. Only a slight increase in the value was observed with the addition of the number of walls. Liang et al.[37] pointed out that the transmission coefficient in the acoustic mismatch model is decreased when the thickness of the solid is shorter than the phonon mean free path owing to the specular reflection at the surface. Also, the phonon mean free path of graphene in the cross-plane direction is much higher than the highest thickness used in this study.[38] Thus, the slight increase in the Kapitza resistance with the number of CNT walls can be associated with the high phonon mean free path of graphene compared to the present model's wall thickness. A similar result was observed for the graphene−water system in which the Kapitza resistance is nearly independent of the number of graphene layers.[11]

Figure 5 shows the effect of water flow through an armchair (10,10) CNT on the Kapitza resistance/length. The inset shows the average velocities as a function of applied external accelerations. The acceleration varied from 0 to 5×10^{11} m/s^2, and the obtained average velocities are in the linear response regime. It is found that the flow of water does not influence the Kapitza resistance. The water density peak and the area density

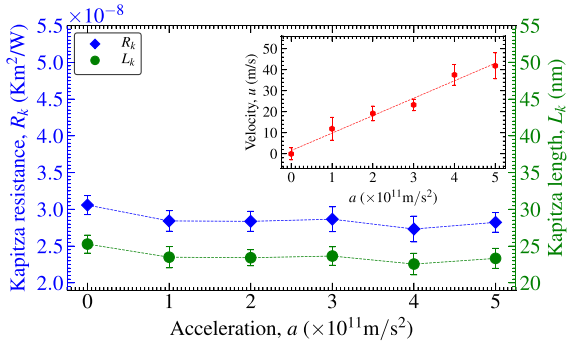


Figure 5. Kapitza resistance/length as a function of different external force fields. The inset shows the average velocity of water along the axial direction of the CNT as a function of external force field.

https://dx.doi.org/10.1021/acs.langmuir.0c03298
Langmuir 2021, 37, 2355−2361

factor, F_{NA} (both are proportional since the diameter is the same), remain unchanged even after applying the external acceleration.[39] Also, there is no noticeable change in the average water temperature due to viscous heating within this range of applied accelerations (see the Supporting Information). Thus, the Kapitza resistance also remains unchanged within the linear response flow regime. Even though we note that our method is strictly true only at equilibrium, it appears to work quite well in the linear response flow regime. The system is in a nonequilibrium state due to the flow; however, we found that the governing parameters of heat flux and temperature difference fluctuate about zero even under the applied external accelerations (see the Supporting Information). Thus, as long as the governing parameters are not far from equilibrium, our method can be used in flow conditions as well. The statistics of the results obtained for systems with flow conditions using the present method is shown to be highly reliable. However, we note that the NEMD method cannot be used to calculate the Kapitza resistance for confined fluids under flow conditions, even in planar systems. This is because the NEMD method requires a steady-state linear temperature profile across the interface, which is impossible to attain when there is flow in the system.

CONCLUSIONS

In summary, we have investigated the nanoconfinement effects on Kapitza resistance at a CNT−water interface using EMD and NEMD methods. We proposed a new EMD method to compute the Kapitza resistance in cylindrical nanoconfinement systems. We find that the NEMD method is not suitable for cylindrical confinement systems under flow conditions (even in planar geometry). We also find that due to the plateau problem that exists in the Green−Kubo-based EMD methods, the Kapitza resistance calculated is highly uncertain and not reliable at higher correlation times. In contrast, our new EMD method is independent of the correlation time, which eliminates the need for selecting any particular and arbitrary correlation time. After validating our method, we studied different factors influencing the Kapitza resistance in a CNT−water system such as diameter, chirality, number of walls, and flow. The CNT diameter is a significant determining factor of the Kapitza resistance. It is found that with an increase in the diameter, the Kapitza resistance decreases and reaches asymptotically near the value of the planar graphene−water interface. Nearly a 56% reduction is obtained when the diameter increased from 1.36 to 6.78 nm. Even though the first density peak of water is higher in the highest diameter CNT, the number of molecules per surface area is lowest due to the cylindrical geometry, which leads to less heat transfer and high Kapitza resistance. Also, the VDOS overlap of the CNT and the water slab adjacent to the interface increases with an increase in the CNT diameter. The area density factor and the VDOS overlap explains the reason for the reduction of the Kapitza resistance with an increase in the CNT diameter. The Kapitza resistance has only a slight influence on the number of walls and is nearly independent of the CNT's chirality. We also find that the flow of water inside the CNT does not have a significant effect on the heat transfer between the CNT and water in the linear flow regime. Unlike the NEMD method, our EMD method is suitable for determining the Kapitza resistance in systems with flow conditions within the linear response regime.

ASSOCIATED CONTENT

Supporting Information

The Supporting Information is available free of charge at https://pubs.acs.org/doi/10.1021/acs.langmuir.0c03298.

Modeling details and the methodology, the simulation details and radial temperature profiles of the NEMD method, the correlation functions and the simulation details of our EMD method, the density profiles of water inside the CNT for different diameters, the calculation of VDOS, the normalized instantaneous heat flux and the normalized instantaneous temperature difference for different accelerations, the variation of area density factor, F_{NA}, and the average temperature of water for different accelerations (PDF)

AUTHOR INFORMATION

Corresponding Author

B. D. Todd − *Department of Mathematics, School of Science, Swinburne University of Technology, Melbourne, Victoria 3122, Australia;* orcid.org/0000-0003-4683-5719; Email: btodd@swin.edu.au

Authors

Sobin Alosious − *Department of Applied Mechanics, Indian Institute of Technology Madras, Chennai 600036, India; Department of Mathematics, School of Science, Swinburne University of Technology, Melbourne, Victoria 3122, Australia;* orcid.org/0000-0003-3579-4747

Sridhar Kumar Kannam − *Department of Mathematics, School of Science, Swinburne University of Technology, Melbourne, Victoria 3122, Australia*

Sarith P. Sathian − *Department of Applied Mechanics, Indian Institute of Technology Madras, Chennai 600036, India;* orcid.org/0000-0003-2756-7210

Complete contact information is available at: https://pubs.acs.org/10.1021/acs.langmuir.0c03298

Notes

The authors declare no competing financial interest.

ACKNOWLEDGMENTS

The authors acknowledge the Swinburne supercomputing OzSTAR facility for providing computational resources for this work.

REFERENCES

(1) Das, S. K.; Choi, S. U.; Yu, W.; Pradeep, T. *Nanofluids: Science and Technology*; John Wiley & Sons, 2007.

(2) Chen, X.; Cao, G.; Han, A.; Punyamurtula, V. K.; Liu, L.; Culligan, P. J.; Kim, T.; Qiao, Y. Nanoscale fluid transport: size and rate effects. *Nano Lett.* **2008**, *8*, 2988−2992.

(3) Thomas, J. A.; McGaughey, A. J. Reassessing fast water transport through carbon nanotubes. *Nano Lett.* **2008**, *8*, 2788−2793.

(4) Majumder, M.; Chopra, N.; Hinds, B. J. Mass transport through carbon nanotube membranes in three different regimes: ionic diffusion and gas and liquid flow. *ACS Nano* **2011**, *5*, 3867−3877.

(5) Kannam, S. K.; Todd, B.; Hansen, J. S.; Daivis, P. J. How fast does water flow in carbon nanotubes? *J. Chem. Phys.* **2013**, *138*, No. 094701.

(6) Li, Q.; Liu, C.; Fan, S. Thermal boundary resistances of carbon nanotubes in contact with metals and polymers. *Nano Lett.* **2009**, *9*, 3805−3809.

(7) Gulotty, R.; Castellino, M.; Jagdale, P.; Tagliaferro, A.; Balandin, A. A. Effects of functionalization on thermal properties of single-wall and multi-wall carbon nanotube-polymer nanocomposites. *ACS Nano* **2013**, *7*, 5114−5121.
(8) Bui, K.; Duong4, H. M.; Striolo, A.; Papavassiliou, D. V. Effective heat transfer properties of graphene sheet nanocomposites and comparison to carbon nanotube nanocomposites. *J. Phys. Chem. C* **2011**, *115*, 3872−3880.
(9) Jabbari, F.; Rajabpour, A.; Saedodin, S.; Wongwises, S. Effect of water/carbon interaction strength on interfacial thermal resistance and the surrounding molecular nanolayer of CNT and graphene flake. *J. Mol. Liq.* **2019**, *282*, 197−204.
(10) Unnikrishnan, V.; Banerjee, D.; Reddy, J. Atomistic-mesoscale interfacial resistance based thermal analysis of carbon nanotube systems. *Int. J. Therm. Sci.* **2008**, *47*, 1602−1609.
(11) Alosious, S.; Kannam, S. K.; Sathian, S. P.; Todd, B. Prediction of Kapitza resistance at fluid-solid interfaces. *J. Chem. Phys.* **2019**, *151*, No. 194502.
(12) Alosious, S.; Kannam, S. K.; Sathian, S. P.; Todd, B. Kapitza resistance at water-graphene interfaces. *J. Chem. Phys.* **2020**, *152*, No. 224703.
(13) Puech, L.; Bonfait, G.; Castaing, B. Mobility of the 3He Solid-Liquid Interface: Experiment and Theory. *J. Low Temp. Phys.* **1986**, *62*, 315.
(14) Barrat, J.-L.; Chiaruttini, F. Kapitza resistance at the liquid-solid interface. *Mol. Phys.* **2003**, *101*, 1605−1610.
(15) Hansen, J. S.; Todd, B.; Daivis, P. J. Prediction of fluid velocity slip at solid surfaces. *Phys. Rev. E* **2011**, *84*, No. 016313.
(16) Evans, D. J.; Morriss, G. *Statistical Mechanics of Nonequilibrium Liquids*; Cambridge University Press, 2008.
(17) Todd, B. D.; Daivis, P. J. *Nonequilibrium Molecular Dynamics: Theory, Algorithms and Applications*; Cambridge University Press, 2017.
(18) Todd, B. D.; Daivis, P. J.; Evans, D. J. Heat flux vector in highly inhomogeneous nonequilibrium fluids. *Phys. Rev. E* **1995**, *51*, No. 4362.
(19) Berendsen, H.; Grigera, J.; Straatsma, T. The missing term in effective pair potentials. *J. Phys. Chem.* **1987**, *91*, 6269−6271.
(20) Wu, Y.; Tepper, H. L.; Voth, G. A. Flexible simple point-charge water model with improved liquid-state properties. *J. Chem. Phys. A* **2006**, *124*, No. 024503.
(21) Ryckaert, J.-P.; Ciccotti, G.; Berendsen, H. J. Numerical integration of the cartesian equations of motion of a system with constraints: molecular dynamics of n-alkanes. *J. Comput. Phys.* **1977**, *23*, 327−341.
(22) Hockney, R. W.; Eastwood, J. W. *Computer Simulation Using Particles*; CRC Press, 1988.
(23) Ostler, D.; Kannam, S. K.; Daivis, P. J.; Frascoli, F.; Todd, B. Electropumping of water in functionalized carbon nanotubes using rotating electric fields. *J. Phys. Chem. C* **2017**, *121*, 28158−28165.
(24) Stuart, S. J.; Tutein, A. B.; Harrison, J. A. A reactive potential for hydrocarbons with intermolecular interactions. *J. Chem. Phys.* **2000**, *112*, 6472−6486.
(25) Girifalco, L.; Hodak, M.; Lee, R. S. Carbon nanotubes, buckyballs, ropes, and a universal graphitic potential. *Phys. Rev. B* **2000**, *62*, No. 13104.
(26) Werder, T.; Walther, J. H.; Jaffe, R.; Halicioglu, T.; Koumoutsakos, P. On the water- carbon interaction for use in molecular dynamics simulations of graphite and carbon nanotubes. *J. Phys. Chem. B* **2003**, *107*, 1345−1352.
(27) Plimpton, S. Fast parallel algorithms for short-range molecular dynamics. *J. Comput. Phys.* **1995**, *117*, 1−19.
(28) Humphrey, W.; Dalke, A.; Schulten, K. VMD—Visual Molecular Dynamics. *J. Mol. Graphics* **1996**, *14*, 33−38.
(29) Grest, G. S.; Kremer, K. Molecular dynamics simulation for polymers in the presence of a heat bath. *Phys. Rev. A* **1986**, *33*, No. 3628.
(30) Wang, G. J.; Hadjiconstantinou, N. G. Why are fluid densities so low in carbon nanotubes. *Phys. Fluids* **2015**, *27*, No. 052006.
(31) Español, P.; de la Torre, J.; Duque-Zumajo, D. Solution to the plateau problem in the Green-Kubo formula. *Phys. Rev. E* **2019**, *99*, No. 022126.
(32) Alexeev, D.; Chen, J.; Walther, J. H.; Giapis, K. P.; Angelikopoulos, P.; Koumoutsakos, P. Kapitza resistance between few-layer graphene and water: liquid layering effects. *Nano Lett.* **2015**, *15*, 5744−5749.
(33) Wang, G. J.; Hadjiconstantinou, N. G. Molecular mechanics and structure of the fluid-solid interface in simple fluids. *Phys. Rev. Fluids* **2017**, *2*, No. 094201.
(34) Ge, Z.; Cahill, D. G.; Braun, P. V. Thermal conductance of hydrophilic and hydrophobic interfaces. *Phys. Rev. Lett.* **2006**, *96*, No. 186101.
(35) Chen, J.; Zhang, G.; Li, B. Tunable thermal conductivity of $Si_{1-x}Ge_x$ nanowires. *Appl. Phys. Lett.* **2009**, *95*, No. 073117.
(36) Sam, A.; Prasad, V.; Sathian, S. P. Water flow in carbon nanotubes: the role of tube chirality. *Phys. Chem. Chem. Phys.* **2019**, *21*, 6566−6573.
(37) Liang, Z.; Sasikumar, K.; Keblinski, P. Thermal transport across a substrate-thin-film interface: effects of film thickness and surface roughness. *Phys. Rev. Lett.* **2014**, *113*, No. 065901.
(38) Wei, Z.; Ni, Z.; Bi, K.; Chen, M.; Chen, Y. Interfacial thermal resistance in multilayer graphene structures. *Phys. Lett. A* **2011**, *375*, 1195−1199.
(39) Hanasaki, I.; Nakatani, A. Flow structure of water in carbon nanotubes: Poiseuille type or plug-like. *J. Chem. Phys.* **2006**, *124*, No. 144708.

https://dx.doi.org/10.1021/acs.langmuir.0c03298
Langmuir 2021, 37, 2355−2361